Soft Matter

PAPER

View Article Online
View Journal | View Issue

Cite this: *Soft Matter*, 2018, **14**, 4977

Necking and drawing of rubber–plastic bilayer laminates†

Rahul G. Ramachandran,[a] S. Hariharakrishnan,[c] Ronald Fortunato,[a] Steven D. Abramowitch,[b] Spandan Maiti[ab] and Sachin S. Velankar*[ac]

Received 2nd April 2018,
Accepted 20th May 2018

DOI: 10.1039/c8sm00684a

rsc.li/soft-matter-journal

We examine the stretching behavior of rubber–plastic composites composed of a layer of styrene–ethylene/propylene–styrene (SEPS) rubber, bonded to a layer of linear low density polyethylene (LLDPE) plastic. Dog-bone shaped samples of rubber, plastic, and rubber–plastic bilayers with rubber : plastic thickness ratio in the range of 1.2–9 were subjected to uniaxial tension tests. The degree of inhomogeneity of deformation was quantified by digital image correlation analysis of video recordings of these tests. In tension, the SEPS layer showed homogeneous deformation, whereas the LLDPE layer showed necking followed by stable drawing owing to its elastoplastic deformation behavior and post-yield strain hardening. Bilayer laminates showed behavior intermediate between the plastic and the rubber, with the degree of necking and drawing reducing as the rubber : plastic ratio increased. A simple model was developed in which the force in the bilayer was taken as the sum of forces in the plastic and the rubber layers measured independently. By applying a mechanical energy balance to this model, the changes in bilayer necking behavior with rubber thickness could be predicted qualitatively.

1 Introduction

Different types of materials can show qualitatively distinct behaviors under tensile stress. If a bar or rod of an elastomeric material with uniform cross section is pulled, it tends to stretch uniformly with a correspondingly uniform decrease in thickness. This is our common experience with a rubber band which stretches homogeneously even when stretched to many times its original length. Another class of materials such as metals and many polymers develop a necking instability in tension, *i.e.* an initially-uniform sample, post yielding, shows strong strain localization. As a result, the material thins locally at the necked region until it fails.[1] However, necking need not necessarily lead to failure. In materials such as some semi-crystalline or glassy polymers, the neck stabilizes and spreads by recruiting new material into the necked region, which is indicative of post-yield strain hardening.[2,3] For example, Fig. 1a shows such behavior in polyethylene, discussed later. Such a material behavior, where deformation proceeds by neck propagation, is called stable drawing or cold drawing, a term originally introduced by Carothers and Hill.[4]

Stability of deformation at the neck is governed by the post-yield constitutive response of the material.[5,6] A commonly-used constitutive model to describe the material response in strain hardening materials in tension is $\sigma = K\varepsilon^n$, where σ is the true stress, ε the true strain, and K and n are constitutive parameters.[7] Typically, the value of n for ductile metals is around 0.5 or less.[8] Therefore, for strains exceeding a few percent, these materials show a gentle rise in stress with strain. Since the load bearing capacity of the neck is decreasing with every strain increment, the material is expected to fail by local thinning. In contrast, the polymers capable of cold drawing show a highly non-linear, asymptotic increase in true stress with strain.[5,9] Such a strain hardening behavior would restrict further deformation in the necked region due to the increasing stress increment required for stretching and thereby stabilizing the neck. This type of highly non-linear strain hardening is common in a wide variety of materials, *e.g.* soft tissues,[10] elastomers,[11] or semi-crystalline polymers.[2]

The central concern of this paper is the behavior of composite laminates in which a layer of a cold drawing plastic is bonded to a layer of elastomer. Since cold drawing plastics show stable necking whereas elastomers stretch homogeneously, it is reasonable to expect that rubber–plastic composites would show intermediate behavior. Mechanics of bilayer laminates of metals and elastomers bonded together, where the metal layer exhibits strong post-yield strain localization, have been studied by Li and Suo.[12] Upon stretching under plane strain conditions, the yielding layer (by itself) developed a single neck which failed

[a] *Department of Mechanical Engineering and Material Science, University of Pittsburgh, Pittsburgh, PA, USA*
[b] *Department of Bioengineering, University of Pittsburgh, Pittsburgh, PA, USA*
[c] *Department of Chemical Engineering, University of Pittsburgh, Pittsburgh, PA, USA. E-mail: velankar@pitt.edu; Tel: +1-412-624-9984*

† Electronic supplementary information (ESI) available. See DOI: 10.1039/c8sm00684a

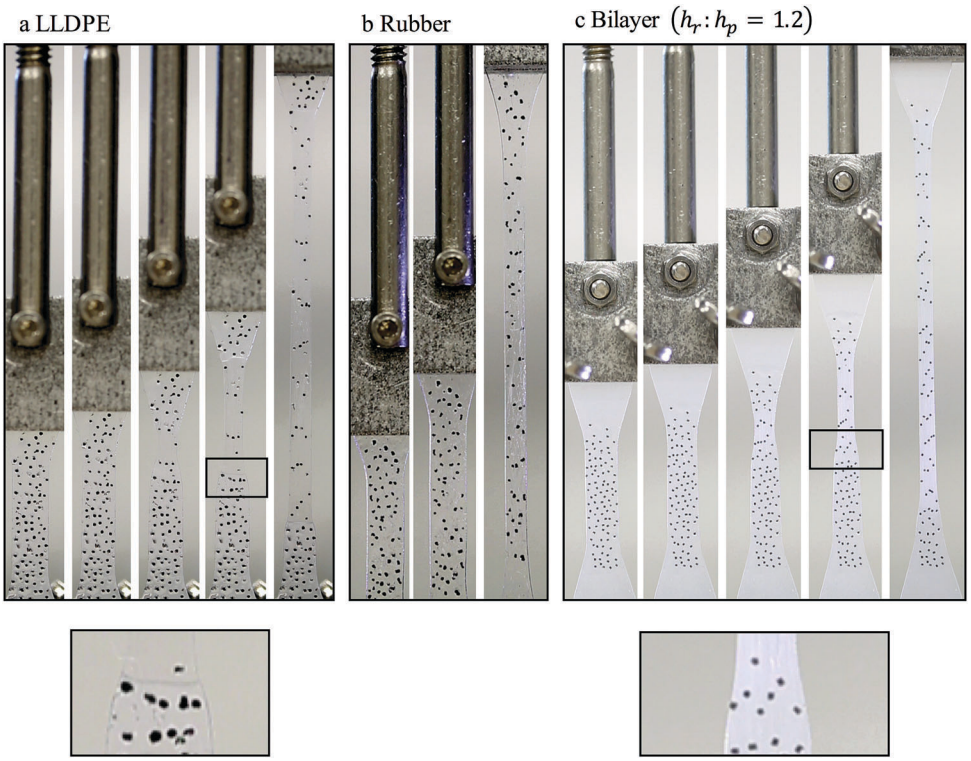

Fig. 1 Images of samples during tensile deformation of dogbone-shaped samples of (a) LLDPE plastic, (b) SEPS rubber, (c) rubber–plastic laminate composite with a 1.2 : 1 rubber : plastic ratio. Black dots are marker particles. Lower two images are magnified view showing the sharp neck of LLDPE and more diffuse neck of the composite. Videos of (a–c) are available as ESI.†

upon further stretching. In contrast, the elastomer (by itself) showed uniform thinning and stretching. Laminate composites with sufficiently large rubber layer thickness or stiffness were predicted to thin homogeneously to large strain. This is interesting because bonding an elastomer allowed a plastic layer (which would ordinarily fail at a small strain by necking) to be stretched to a high strain without failure. Indeed, this situation – the experimental[13,14] and numerical observations[15] that metal films bonded to elastomers could be stretched in a ductile fashion up to a high strain – was the motivation for their research[12] and subsequent research on this topic.[16–26] However, that research was restricted to cases such as metal–rubber composites where the plastic layer (metal) could not show stable drawing. The situation when the plastic layer of the composite is a strain hardening polymer that is capable of stable drawing is likely to be quite different. The goal of this article is to explore the modification of necking and drawing behavior when such a stable drawing polymer is bonded to an elastomer.

An example illustrating the main issues of interest in this paper is shown in Fig. 1 which compares the tensile deformation behavior of a plastic layer, a rubber layer, and a rubber–plastic bilayer laminate composite. Here we will only discuss the qualitative aspects briefly; the quantitative details will be discussed later in this paper. Fig. 1a shows the behavior of a film of linear low-density polyethylene (LLDPE) plastic which develops a neck at a modest deformation, followed by stable drawing during which the necked region grows by recruiting new material into the neck. During stable drawing, neither the necked region nor the material outside the neck deforms significantly. Instead, deformation is confined to a very narrow transition zone (which appears as a sharp line in the images) between the necked and un-necked regions. Fig. 1b shows a sample of styrene–ethylene/propylene–styrene (SEPS) rubber, and in sharp contrast to the LLDPE, the SEPS deforms homogeneously with no indication of any localized stretching. Finally Fig. 1c shows a bilayer laminate composite of the SEPS : LLDPE in the thickness ratio of 1.2 : 1. The behavior is intermediate between the rubber and the plastic: while the sample does undergo necking, the transition between the necked and un-necked region is not as sharp (this is especially clear in the videos, *LLDPE.avi*, *SEPS.avi* and *Bilayer.avi*, available as ESI†), and we will show later that the magnitude of strain localization is reduced as compared to Fig. 1a. In this paper we explore this situation quantitatively and address the extent to which the necking behavior is modified, and how this depends on rubber thickness.

This article is organized as follows. Sections 2.1 and 2.2 respectively describe the experimental procedures and data analysis. The later focuses mainly on converting the images such as Fig. 1 into quantitative strain maps. Section 3.1 examines the force behavior obtained in tensile tests. Section 3.2 discusses the deformation qualitatively, whereas Section 3.3 quantifies the degree of non-uniformity of the deformation as the rubber : plastic ratio is varied. Section 4 develops a simple model of the composite behavior, and also discuss the limitations of the model.

2 Methods

2.1 Experimental

Most of the details of experimental methods are given in the ESI.† Briefly, bilayer laminate samples were prepared by bonding LLDPE films to SEPS rubber films using compression molding. Most of the samples have a nominal plastic layer thickness of 120 μm, whereas a few samples have a nominal plastic layer thickness of 50 μm. 50 μm thick plastic layer was used to achieve large rubber : plastic thickness ratios. Dog-bone shaped samples (6 mm width and a nominal gauge length of 20 mm) were cut from the resulting bilayer composite sheet. Small black particles were then stuck onto this surface (rendered sticky with silicone oil) to serve as markers for Digital Image Correlation (DIC). Tensile testing was conducted at a crosshead speed of 120 mm min^{-1} and video-recorded. The two layers remained fully bonded to each other during tensile deformation (and indeed remained bonded after releasing, causing the plastic layer to develop intense wrinkles[24]). Similar experiments were conducted on the SEPS and the LLDPE layers individually; the ESI† explains how residual orientation of the LLDPE film was relaxed prior to experiments.

2.2 Stretch mapping by DIC

Since the deformation of the samples was not always uniform along its length, the stretch profile on the sample surface was computed for quantifying deformation. A finite element based interpolation technique was used to estimate the evolution of the stretch distribution with time on the sample surface by tracking the position of the finite number of marker points. Typical distribution of the marker particles (the black dots) on the samples can be seen from Fig. 1. Marker positions were tracked at each frame of the recorded video of the specimen deformation by using Blender™ (Stitching Blender Foundation, Amsterdam, Netherlands) software suite. The marker positions from the first video frame was triangulated to construct the reference configuration, which was a 2D finite element mesh of three-noded triangles with nodes located at the marker locations. The marker locations were triangulated by Delaunay triangulation technique by using the opensource software Triangle (Computer Science Division, University of California at Berkeley). Fig. 2 shows examples of the initial reference configuration (Fig. 2a), and the deformed configuration at some later instant (Fig. 2b) for an LLDPE sample, superimposed on the corresponding image.

The stretch map was generated by evaluating the stretch in the axial direction of each triangular element at their corresponding integration point and then averaging them at nodes.[27] The process was repeated at all frames of the video recording to generate the stretch evolution with time, on the sample surface. Calculations involved in obtaining the stretch map are described in ESI.† An example of the stretch maps as a function of time is shown as ESI† video *LLDPE_Stretch_Map.avi*.

Fig. 2c shows the calculated stretch map superimposed onto the image of the deformed specimen of Fig. 2b. Overall the local deformation of the sample is very well-captured by the color maps. Yet, we acknowledge that at the transition between the necked and un-necked region, agreement is much poorer. Specifically, the experimental image shows a sharp transition, whereas the color map appears much smoother. This is because our continuum mechanics based DIC algorithm cannot capture displacement discontinuities arising at the sharp transition fronts.

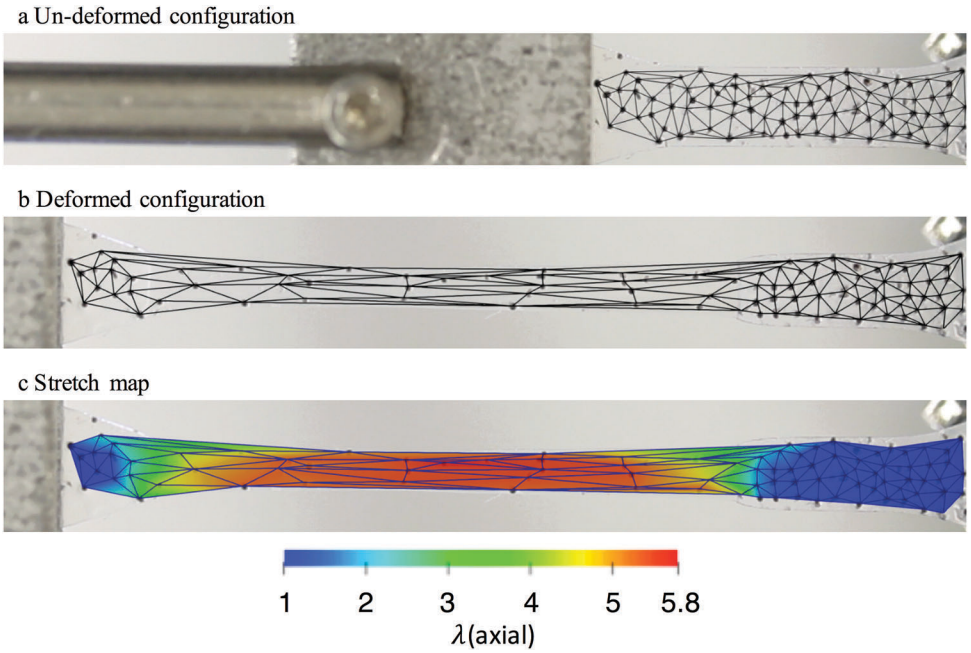

Fig. 2 Mesh generated by triangulating the marker locations superimposed over the corresponding frame of the recorded video in (a) the initial configuration and (b) deformed configuration. (c) The stretch map corresponding to (b).

Increasing the area density of the markers would allow displacement discontinuity at the transition front to be represented as a sharp gradient. Thus, the analysis below will only use the maximum and minimum values of stretch, with no further comment on the sharpness of the transition.

3 Results

3.1 Mechanical behavior of LLDPE/SEPS bilayer

We start with discussing the force data measured during tensile testing experiments (the corresponding videos are discussed in the Section 3.2). Fig. 3a shows the nominal stress strain response of pure LLDPE plastic, SEPS rubber and laminate composites with two different rubber : plastic thickness ratios. Here the nominal strain is defined as the ratio of the crosshead displacement to the gauge length (20 mm). The free-standing LLDPE plastic and the two rubber–plastic bilayer laminates in Fig. 3 all have the same nominal plastic layer thickness of 120 microns. The stress–strain curve for the SEPS rubber increases monotonically. In contrast, the LLDPE plastic shows a sharp rise in stress at small strain, followed by a peak which is generally associated with the onset of neck formation. More specifically, since the neck has a smaller cross-sectional area than the original sample, the total force reduces upon neck initiation, and so does the nominal stress. Since the decrease in nominal stress is primarily attributable to a decrease in cross sectional area at the neck, it is sometimes called geometric softening.[28] The load however does not continue reducing indefinitely. Instead it reaches a minimum value that corresponds to the onset of stable drawing. Then the stress rises gently over a wide range of nominal strain over which the necked region propagates across the entire sample. Once the neck reaches the wider ends of the dog-bone shaped specimen, the nominal stress rises again.

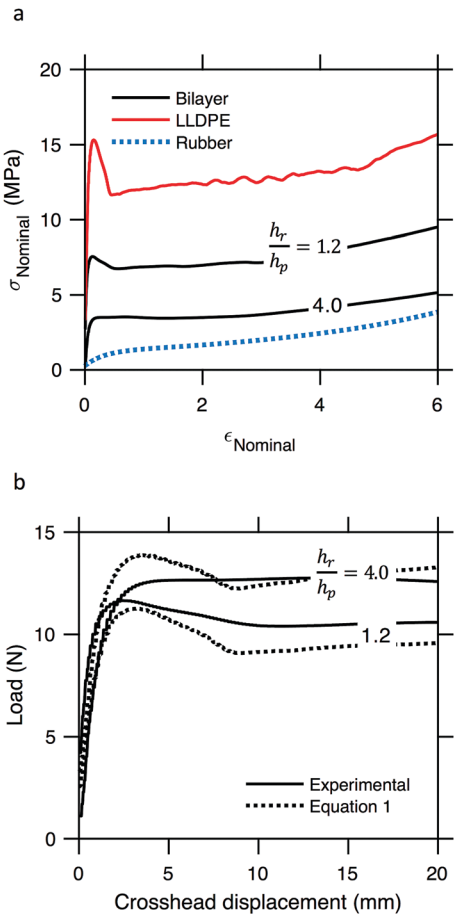

Fig. 3 (a) Nominal stress–strain response for SEPS rubber, LLDPE, and LLDPE–rubber bilayers of rubber : plastic thickness ratio 1.2 and 4.0 stretched at a rate of 120 mm per minute. (b) The same data as the composites in (a) but shown as force *vs.* crosshead displacement. Only the small-deformation region is shown in (b). Dotted lines in (b) are eqn (1).

The behavior of the composites is qualitatively similar to that of the plastic, but with the key difference that the peak is much less sharp. To emphasize the difference between the layered composites *vs.* the LLDPE in the peak region, Fig. 3b plots the same results, but in the form of load–elongation curves at small strain. These measured curves are compared against the simplest model of a layered composite, which is to treat the total force as a sum of the force in each layer:

$$F_{\text{bilayer}} = F_{\text{r}} + F_{\text{p}} = w[h_{\text{r}}\sigma_{\text{nom,r}} + h_{\text{p}}\sigma_{\text{nom,p}}] \quad (1)$$

where h_{r} and h_{p} are the rubber and plastic layer thickness respectively, w is the sample width, and $\sigma_{\text{nom,r}}$ and $\sigma_{\text{nom,p}}$ are the nominal stresses for the rubber and plastic measured independently at the same nominal strain (*i.e.* same crosshead displacement). The predictions of eqn (1) are shown in Fig. 3b as dotted lines. This comparison makes it clear that for both the laminate composites shown, the experimentally-measured peak is much less sharp than predicted by eqn (1). Furthermore, for $h_{\text{r}}/h_{\text{p}} = 4.0$, the force–strain curve shows no apparent peak. Since the presence of a peak is associated with necking, the force data alone suggest that the degree of necking decreases with increasing rubber thickness, which will be considered next.

3.2 Qualitative behavior of tensile deformation

Fig. 4 shows the stretch maps of LLDPE, SEBS rubber, and a rubber–plastic laminate composite. The crosshead displacements for each of the images is listed below the image. The LLDPE initially deforms uniformly (second frame shown in Fig. 4a), followed by necking (evident as the green region with higher stretch in the third frame). With further crosshead displacement, the stretch in the neck first increases, but eventually (last two frames in Fig. 4a) it saturates as judged by the similar intensity of the red color in the last two frames. Beyond this point, further crosshead displacement is accommodated purely by drawing un-necked material into the neck, with no further change in the necked region.

In sharp contrast, the rubber (Fig. 4b) stretches uniformly, as judged by the nearly uniform color at all deformation stages, with the stretch increasing steadily with crosshead displacement.

The behavior of LLDPE–rubber bilayer with $h_{\text{r}}/h_{\text{p}} = 1.2$ (Fig. 4c) is qualitatively similar to that of the LLDPE: the initial deformation is homogeneous, followed by necking and then drawing. The chief difference is that the maximum stretch

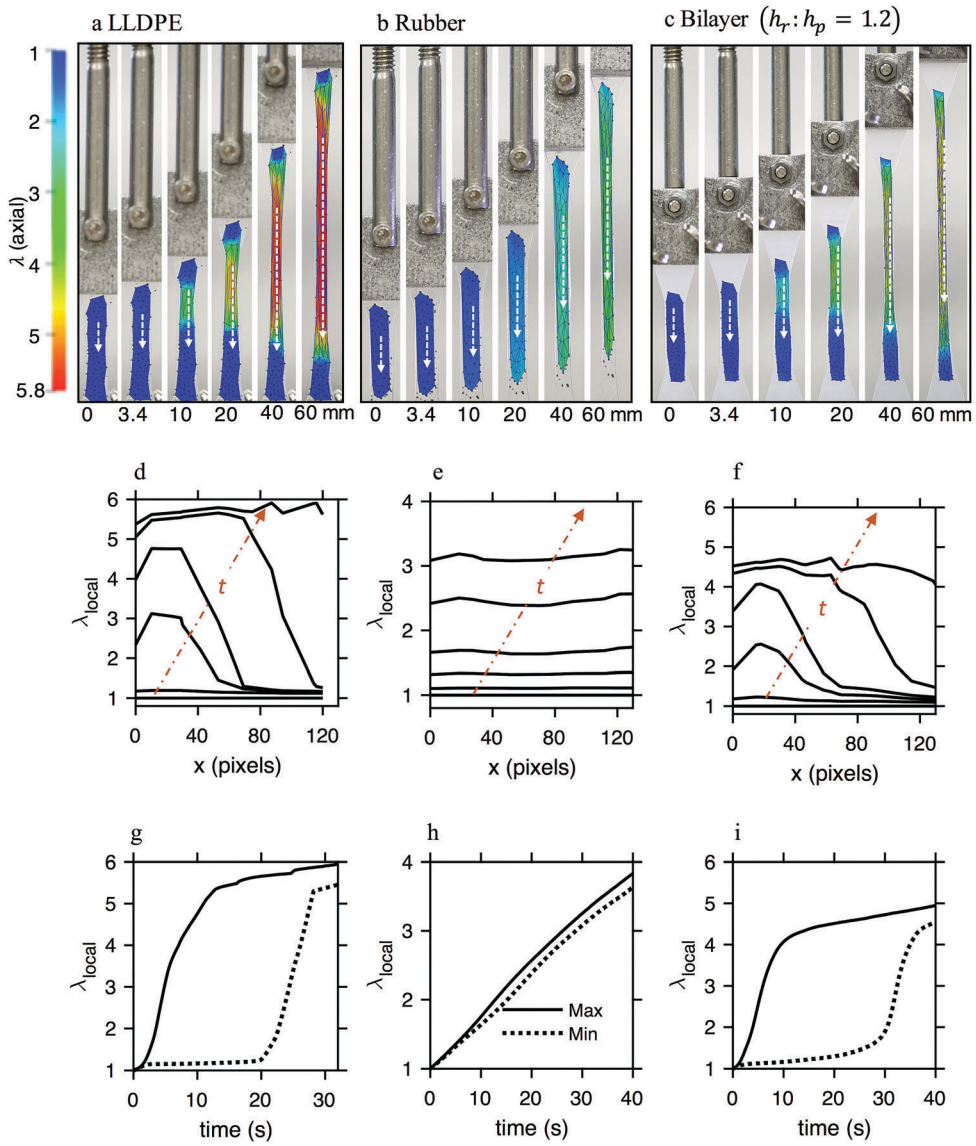

Fig. 4 (a–c) Stretch maps superimposed on corresponding specimen configurations for (a) LLDPE plastic, (b) SEPS rubber, (c) bilayer composite with rubber : plastic thickness ratio of 1.2. The number below each image is the crosshead displacement. (d–f) Plots of stretch data extracted along the white dashed lines in (a–c) plotted against the pixel coordinate along the line in the undeformed configuration. (g–i) Maximum and minimum stretches *vs.* time along the white dashed lines in (a–c).

developed in the necked region saturates at a much lower value than the LLDPE. Accordingly, towards the end of the stretching experiment, the neck propagates throughout the test section of the sample, and hence the deformation reverts to becoming homogeneous. The electronic Fig. S1a and b (ESI†) shows stretch maps for two other rubber : plastic thickness ratios (2.4 and 4.0). At a ratio of 2.4, the behavior is qualitatively similar to Fig. 4c. At a ratio of 4.0, the necking behavior is much more subtle; variations in stretch across the length of the test section remain relatively small (albeit larger than the SEPS rubber in Fig. 4b) throughout the experiment.

3.3 Quantifying inhomogeneous deformation

We now proceed with a more quantitative analysis. Since the deformation of the samples is predominantly uniaxial, most of the insights about the heterogeneity of sample deformation can be obtained from examining the stretch along the stretching direction only. Accordingly, the stretch was extracted along the center line in the gauge section of the dog-bone as illustrated by the dashed lines in Fig. 4a–c. Therefore, these dotted lines are the region of interest (ROI) for quantitative analysis. The end-points of these lines were chosen to ensure that the transition from the un-necked to the necked region could be followed unambiguously, while still avoiding the wider ends of the dog-bone shaped specimen. The stretch profiles along the centerline for the samples of Fig. 4a–c are shown in Fig. 4d–f respectively. In these plots, the abscissa indicates the location (in pixels) along the dashed lines, whereas the ordinate axis shows the corresponding axial stretch at that location (λ_{local}). These plots now quantify all the features discussed in the

previous section. The LLDPE (Fig. 4d) shows necking, followed by drawing, with the stretch saturating at roughly 5.7. This value can be regarded as the natural draw ratio of this LLDPE, defined as the steady state stretch at which the neck stabilizes for a cold drawing plastic.[2] The rubber sample (Fig. 4e) shows a monotonic increase in stretch, but with little spatial variation with position at any instant. The composite laminate (Fig. 4f) with rubber : plastic thickness ratio 1.2 behaves similarly as the LLDPE, but with the stretch saturating at roughly 4.5.

As a quantitative measure of the degree of heterogeneity in the deformation, we extract the maximum and minimum stretch, λ_{max} and λ_{min} at all stages of deformation for each sample. Fig. 4g–i plot these extreme values for each of the three samples of Fig. 4a–c throughout the deformation. Fig. S1c and d in the ESI† plots the same for bilayers of rubber : plastic thickness ratio 2.4 and 4.0.

To facilitate comparisons of the various samples, Fig. 5a plots λ_{max} *vs.* λ_{avg}, where λ_{avg} is the average stretch in the ROI. Fig. 5a includes all the three samples of Fig. 4 as well as bilayer laminates with two additional thickness ratios shown in the Fig. S1 (ESI†). The degree of non-homogeneity of deformation can be readily identified from this plot as deviations from the $\lambda_{max} = \lambda_{avg}$ line. For the SEPS rubber, the data remain close to the $\lambda_{max} = \lambda_{avg}$ line throughout the deformation indicating near-homogeneous deformation. All the other samples deviate from the $\lambda_{max} = \lambda_{avg}$ line, with deviations becoming more severe as the rubber thickness decreases. Furthermore, samples with small rubber thickness show a near plateau in λ_{max} whose value is the natural draw ratio. In contrast, the sample with $h_r/h_p = 4.0$, λ_{max} shows a steady increase during the deformation. This implies that there is no stable drawing regime, and one cannot identify a single value as a natural draw ratio.

It would be convenient to have a single numerical metric to quantify the degree of non-homogeneity of deformation. The most convenient metric for this purpose would be the plateau in λ_{max} because it has immediate physical significance as the natural draw ratio. Yet, the λ_{max} plateau is not an ideal metric because at large rubber thickness, the data do not show a plateau at all. Furthermore, Fig. 4f, and Fig. S1c, d (ESI†) all show that λ_{min} itself increases indicating that the non-homogeneity of deformation reduces during the deformation process. Ideally, we would prefer a metric that can capture the changes in both λ_{max} and λ_{min}. One simple approach is to take the ratio $\lambda_{max}/\lambda_{min}$. This quantity is plotted against λ_{avg} in Fig. 5b. We may now select any convenient average stretch and use the corresponding value of $\lambda_{max}/\lambda_{min}$ to quantify the degree of non-homogeneity. For instance, the dashed line in Fig. 5b shows $\lambda_{avg} = 3.5$, and the corresponding values of $\lambda_{max}/\lambda_{min}$ are plotted in Fig. 7a.

We acknowledge that the choice of $\lambda_{avg} = 3.5$ is arbitrary, and a different choice of λ_{avg} would give somewhat different values for $\lambda_{max}/\lambda_{min}$. For instance, ESI† Fig. S2 shows $\lambda_{max}/\lambda_{min}$ at $\lambda_{avg} = 3$, and the points at high rubber thickness are distinctly shifted with respect to Fig. 7a.

To avoid this arbitrariness, we define a new metric, dubbed the inhomogeneity index, as the highest value of $\lambda_{max}/\lambda_{min}$ during the entire deformation. Thus, the inhomogeneity index is the *y*-axis value of the open circles in Fig. 5b. These values of the inhomogeneity index are plotted in Fig. 7b as a function of the rubber : plastic thickness ratio. Both Fig. 7a and b show similar trends: the non-homogeneity of deformation reduces as rubber thickness increases.

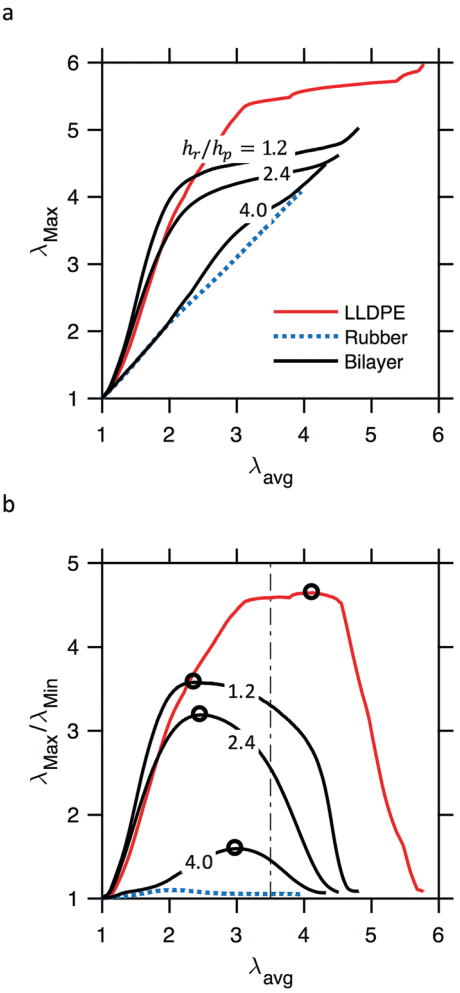

Fig. 5 (a) Maximum stretch *vs.* average stretch in the ROI, for a free-standing LLDPE, a free-standing SEPS and bilayer laminates of rubber : plastic thickness ratio 1.2, 2.4 and 4.0 (b) same samples as in (a), but with maximum to minimum stretch ratio plotted against average stretch in the ROI. The maximum of each curve, indicated with an open circle, is defined as the inhomogeneity index. The dot-dashed line corresponds to an average stretch of 3.5.

4 Discussion

To summarize the main experimental observations: tensile behavior of the LLDPE plastic is characterized by necking, followed by stable drawing, and a sharp transition between the necked and un-necked zone. Once stable drawing is realized, the natural draw ratio in the necked region is roughly 5.7, whereas the un-necked region is nearly undeformed (stretch of about 1.1).

Composites of the LLDPE plastic and the SEPS rubber show the following features: decrease in the stretch of the necked region; an increase in the stretch of the un-necked region; and an increase in the width of transition between the necked and un-necked region. In some cases, the necked region reaches the wider ends of the dog-bone shaped sample, therefore the deformation in the sample reverts to being uniform across the entire sample.

The remainder of this discussion is split into two sections. The first develops a simple model that captures many of the experimental observations. The second discusses possible refinements and limitations of the model along with other noteworthy issues.

4.1 Force-additive rule of mixtures model

The overall goal of the model is not a detailed description of deformation, but a minimal description that captures most of the above observations. The analysis is based on the following assumptions. The first is eqn (1), that the force developed in the bilayer is simply the sum of the force in the plastic and the rubber layers measured independently at the same crosshead displacement. This is equivalent to assuming that the two layers are not bonded to each other, but simply deforming in parallel. We will comment further on this assumption at the end of this section, but Fig. 3b suggests that – despite the difference in the sharpness of the peak in the stress strain curve – eqn (1) is reasonably correct. The second assumption is to ignore the transition region between the necked and un-necked regions. Thus, a sample can have at most two values of stretch that coexist at any instant. Finally, we adopt the simplest constitutive models that capture the qualitative behavior of the individual layers. For the rubber, a two parameter Mooney Rivlin hyperplastic constitutive relation was found to capture the rubber behavior reasonably well. For uniaxial deformation, the corresponding nominal stress is given by,

$$\sigma_{\mathrm{nom,r}} = 2\left(C_{1,\mathrm{r}} + \frac{C_{2,\mathrm{r}}}{\lambda}\right) \times \left(\lambda - \frac{1}{\lambda^2}\right) \qquad (2)$$

The values of $C_{1,\mathrm{r}}$ = 0.305 MPa and $C_{2,\mathrm{r}}$ = 0.360 MPa were found by fitting the measured data for the SEPS rubber. We note that setting $C_{2,\mathrm{r}}$ = 0 reverts to the simpler neo-Hookean model, but this gave poor fits to the measured SEPS rubber data.

The plastic behavior is approximated by a two-parameter model previously employed by Haward to describe the behavior of a wide variety of thermoplastics.[29] In Haward's approach, the stress in the LLDPE is assumed to be sum of a yield stress and incompressible neo-Hookean stress:

$$\sigma_{\mathrm{nom,p}} = \frac{\sigma_{\mathrm{yield}}}{\lambda} + 2C_{1,\mathrm{p}} \times \left(\lambda - \frac{1}{\lambda^2}\right) \qquad (3)$$

This model has the obvious shortcoming that the stress has a discontinuity at zero strain, and hence mechanical behavior prior to yielding cannot be captured. Nevertheless, this model provides a simple analytical approach to quantify necking and drawing behavior. The yield stress (σ_{yield}) of LLDPE was taken to be the peak stress in the experimental nominal stress stretch curve and assigned a value of 16.8 MPa which is an average from multiple specimens. The $C_{1,\mathrm{p}}$ value was obtained as

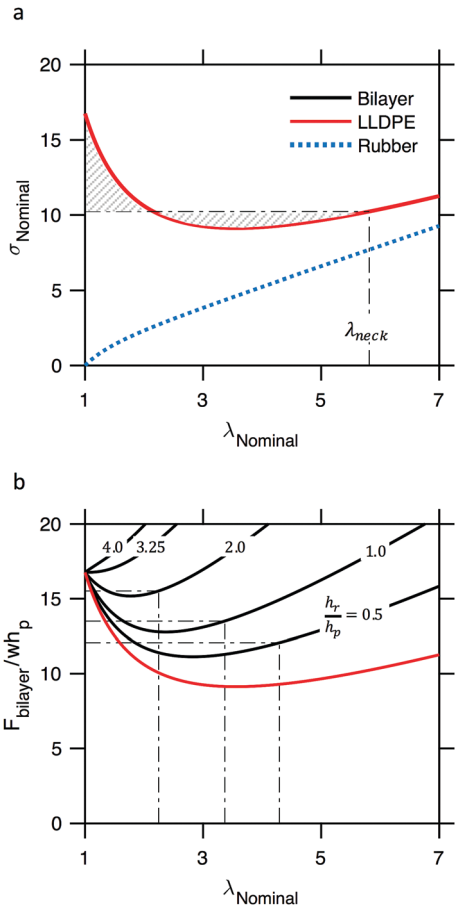

Fig. 6 (a) Constitutive behavior of SEPS and LLDPE approximated by eqn (2) and (3) respectively. The black dot-dashed line is the Maxwell line construction where the shaded areas are equal. (b) Solid black lines are predictions of eqn (9) for the various rubber : plastic ratios indicated. Solid red line is the LLDPE behavior, same curve as in (a). Horizontal dot-dashed lines are Maxwell constructions for each rubber : plastic ratio.

follows. As per the mathematical form of eqn (3), in a tensile experiment, the sample yields at λ = 1 once the yield stress is exceeded. The subsequent behavior depends on the value of $C_{1,\mathrm{p}}$. For $2C_{1,\mathrm{p}} > \sigma_{\mathrm{yield}}/3$, the nominal stress increases monotonically with stretching. In contrast, for $2C_{1,\mathrm{p}} < \sigma_{\mathrm{yield}}/3$, the nominal stress first reduces and then increases at high stretch (see Fig. 6a). The latter must be true for LLDPE because non-monotonic behavior of the nominal stress–stretch relationship is necessary to see necking. The natural draw ratio then depends on the subsequent rise of the nominal stress at high stretch. One approach to calculating the natural draw ratio from the $\sigma_{\mathrm{nom,p}}(\lambda)$ was provided by the Maxwell equal area construction as described by Hutchinson *et al.*[9] The construction is shown in Fig. 6a as a black dashed horizontal line drawn such that the two closed areas between the dotted line and the stress–stretch curve are equal. The idea is derived from the fact that as a material point transforms from an un-necked region to a necked region, the work done by the applied force must equal the change in energy in the material:

$$\sigma_{\mathrm{draw}}(\lambda_{\mathrm{neck}} - \lambda_{\mathrm{unneck}}) = W_{\mathrm{neck}} - W_{\mathrm{unneck}} \qquad (4)$$

where λ_{neck} is the stretch corresponding to the necked region, *i.e.* the natural draw ratio, λ_{unneck} is the stretch corresponding to the region that has not yet necked, and σ_{draw} is the nominal stress corresponding to stable drawing called draw stress. Since the constitutive behavior of eqn (3) gives yielding and neck initiation at $\lambda_{unneck} = 1$, we have $W_{unneck} = 0$. This implies

$$\sigma_{draw}(\lambda_{neck} - 1) = W_{neck} \tag{5}$$

where,

$$W_{neck} = \int_1^{\lambda_{neck}} \sigma_{nom,p}(\lambda)d\lambda = \ln(\lambda_{neck}) + 2C_{1,p}\left\{\frac{{\lambda_{neck}}^2 - 1}{2} + \left(\frac{1}{\lambda_{neck}} - 1\right)\right\} \tag{6}$$

Moreover, since the stress for drawing is simply the nominal stress corresponding to the necked region,

$$\sigma_{draw} = \sigma_{nom,p}(\lambda_{neck}) = \frac{\sigma_{yield}}{\lambda_{neck}} + 2C_{1,p}\left(\lambda_{neck} - \frac{1}{{\lambda_{neck}}^2}\right) \tag{7}$$

Since $\sigma_{yield} = 16.8$ MPa and $\lambda_{neck} = 5.7$ is already known, we can combine eqn (5)–(7) to find $C_{1,p}$ explicitly:

$$C_{1,p} = \frac{\sigma_{yield}\left\{\ln(\lambda_{neck}) + \frac{1}{\lambda_{neck}} - 1\right\}}{{\lambda_{neck}}^2 - 2\lambda_{neck} + 2\frac{1}{{\lambda_{neck}}^2} + 3} \tag{8}$$

The value of $C_{1,p}$ thus calculated is 0.635 MPa. Incidentally, with this value for $C_{1,p}$, eqn (7) predicts $\sigma_{draw} = 10.2$ MPa, which underestimates the measured value of roughly 13.7 MPa. We will comment on this later.

The rule of mixture as given by eqn (1) can now predict the behavior of the bilayer. For convenience the bilayer force is normalized by the undeformed cross-sectional area of the plastic layer:

$$\frac{F_{bilayer}}{wh_p} = \frac{h_r}{h_p}\sigma_{nom,r} + \sigma_{nom,p} \tag{9}$$

Note that although the left-hand side in eqn (9) has units of stress, it does not represent the stress at any physical location; it is simply a convenient way of normalizing the force. Eqn (9) is plotted in Fig. 6b using the constitutive parameters already determined, for various values of h_r/h_p. It is clear that for large rubber thicknesses, the force *vs.* stretch curve is monotonic, and hence necking is not expected. For $h_r/h_p < 3.25$, the force *vs.* stretch curve has a minimum and hence necking is expected. Similar to the free-standing plastic, eqn (3) also shows yield at $\lambda = 1$, *i.e.* the model predicts that the undrawn portion of the bilayer laminates is completely undeformed, and $\lambda_{unneck} = 1$. The draw ratio for the bilayer laminates can then be found numerically from the Maxwell equal area construction which can now be compared against experiments.

In fact, it is difficult to compare the draw ratio against experiments directly. This is because at large rubber thicknesses, the maximum stretch λ_{max} in the necked region does not show a plateau (Fig. 5a), so a single unique draw ratio is difficult to identify. Therefore, we compare the model against the two measures of non-homogeneity of deformation discussed in Section 3.2: the ratio $\lambda_{max}/\lambda_{min}$ obtained at $\lambda_{avg} = 3.5$ (Fig. 7a) and the inhomogeneity index (Fig. 7b). For the model described, the value for comparison is simply $\lambda_{neck}/\lambda_{unneck} = \lambda_{neck}$. The corresponding comparisons shows reasonable agreement with the experimental quantification of inhomogeneity at low rubber thicknesses, but not at large rubber thicknesses. Specifically, the model predicts that necking is eliminated for $h_r/h_p > 3.25$, whereas significant inhomogeneous deformation is still evident at larger values of rubber thickness. Indeed, experimentally we were not able to completely eliminate necking even at the highest rubber thickness examined.

A second parameter of comparison is the draw stress from experiment against model predictions. Experimentally this is simply the nominal stress value corresponding to the onset of stable drawing, which is the local minimum in the nominal stress strain curve post yielding. To obtain the predicted value of the draw stress, the force $F_{bilayer}$ is obtained from eqn (9) where $\sigma_{nom,r}$ and $\sigma_{nom,p}$ are evaluated by substituting the predicted values of λ_{neck} into eqn (2) and (3). The corresponding nominal stress is simply $F_{bilayer}/(wh_r + wh_p)$, and is shown as a solid line in Fig. 7c. The predicted draw stress reduces from 10.2 MPa for the free-standing LLDPE to roughly 4 MPa for $h_r/h_p = 3.25$. Beyond this rubber thickness, the deformation is predicted to be homogeneous and it is not physically meaningful to define a draw stress. Fig. 7c plots the experimentally obtained draw stress with h_r/h_p and compares with predicted values. The draw stress is poorly predicted for pure LLDPE. Fortuitously, the draw stress is in much better agreement for the bilayer laminates. Overall, the trend of decrease in draw stress with increasing rubber thickness is qualitatively captured.

4.2 Limitations

Although very simple, the model appears to be qualitatively successful in capturing the decrease in the inhomogeneity of deformation (Fig. 7a and b) and decrease in the stress for stable drawing (Fig. 7c). Quantitatively however, there are three significant discrepancies. First, the stress for stable drawing for the free-standing plastic is underpredicted by about 25%. Second, the plastic and the composites all yield at a stretch of 1, and hence one important experimental observation, that the onset of necking requires higher stretch for the laminate composites, is not captured even qualitatively. Finally, the model predicts that deformation is homogeneous for $h_r/h_p > 3.25$ whereas experimentally, deformation remains somewhat inhomogeneous even at the highest rubber : plastic thickness ratios examined.

Some these limitations may be addressed with a constitutive equation for the plastic layer that accounts for elastic behavior up to some finite strain prior to yield. Yet, even with this improvement, the above modeling approach may not be able to capture the experimental observations quantitatively for several reasons. First, eqn (1) treats the bilayer force as a sum of the force in the rubber and in the plastic when measured independently. Yet, when tested independently, the plastic undergoes necking whereas the rubber does not, and hence they are in an altogether different strain state. In a bilayer composite, since the layers are

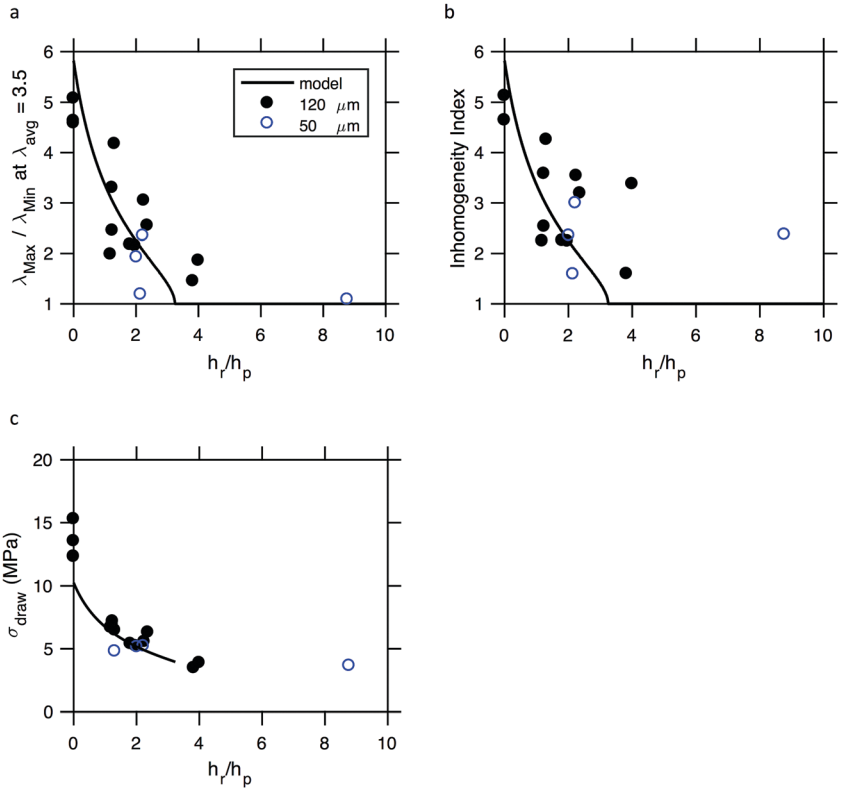

Fig. 7 (a) Ratio of maximum stretch to minimum stretch in ROI, when the average stretch in ROI is 3.5 (b) inhomogeneity index and (c) draw stress, all plotted *vs.* rubber : plastic thickness ratio. Filled and open circles are bilayers with 120 micron and 50 micron plastic respectively. Solid lines are model predictions.

bonded, their strain state must be very similar. As one consequence, at small rubber thicknesses, the rubber layer in the necked region experiences a stretch that far exceeds that in the free-standing rubber. In the other extreme, at large rubber thicknesses when deformation is homogeneous, the plastic layer experiences a variety of strain states, whereas the free-standing plastic is mostly in just two states – necked ($\lambda \sim 5.7$) or un-necked ($\lambda \sim 1$). This fact – that in the bilayer each layer constrains the deformation of the other – affects the width-direction narrowing of the samples as well. Clearly then, the individual layers in the bilayer may experience very different strain from the corresponding free-standing layer, which is not captured in eqn (1). Second, the equal-area analysis is based on treating the behavior of the plastic as a non-linearly elastic material, *i.e.* eqn (5) is a statement of energy conservation during deformation. In fact, the plastic deforms permanently, and energy is not conserved. Finally, one key observation is that the transition zone between the necked and un-necked region is sharp for the free-standing plastic, but becomes much broader as rubber thickness increases. Obviously since the model of the previous section altogether ignores the transition zone, this broadening cannot be captured at all. In fact, the transition region is the only region that actually deforms during stable drawing, and hence it is not possible to correctly describe drawing (neither for the free-standing plastic layer nor for the bilayer) without explicitly modeling the transition region.[30] We are presently conducting FEM simulations, to be published, which address the deficiencies of the 1D model.

One last noteworthy aspect is sample-to-sample variability in the experiments. The SEPS rubber was found to deform homogeneously in all cases, whereas the LLDPE samples showed highly consistent necking and drawing, with the natural draw ratio λ_{max} being close to 5.7 in all cases. In contrast, the bilayers showed much greater variability as may be judged from Fig. 7 despite no apparent differences in sample quality or sample thickness. A possible reason for this may be judged from Fig. 6b which shows that slightly below the value of $h_r/h_p = 3.25$, the force *vs.* stretch curve must necessarily have a very shallow minimum. In such cases, while necking is possible, imperfections in the experiment may affect whether a neck develops, and how severely. Such imperfections include minor mis-misalignment of the dog-bone shaped specimen with respect to the stretching direction, small stresses imposed during loading the sample, or variations in layer thickness within each sample.

5 Summary and conclusion

We examined the tensile behavior of bilayer laminate films of SEPS rubber and LLDPE plastic with rubber : plastic ratios ranging from 1.2 to 9. Similar to many semi-crystalline polymers, LLDPE when stretched shows necking at a few percent strain

owing to plastic yielding, followed by stable drawing owing to its strong strain hardening character, post-yield. In contrast, the elastomer does not exhibit plastic deformation and hence stretches uniformly, similar to most hyperelastic materials. Dog-bone shaped specimens prepared by compression molding were subjected to tensile tests, and the degree of non-homogeneity in the deformation field was quantified by digital correlation image analysis of video recordings of the tensile tests. Bilayer laminates showed behavior that was intermediate between the plastic and the rubber. Bilayers with thin rubber layers showed necking and drawing, but the stretch of the necked region (*i.e.* the natural draw ratio) was lower than of the free-standing plastic. Moreover, the transition between the necked and un-necked region was also much less sharp than in the LLDPE plastic. At large rubber thickness, necking was almost completely eliminated, although the deformation was not completely homogeneous even at the largest rubber : plastic thickness ratio examined.

A simple model was developed in which the force in the bilayer was taken as the sum of forces in the plastic and the rubber layers measured independently. Mechanical energy balance based on the Maxwell construction, was applied to this model to predict how the rubber layer affects necking and drawing. The model successfully predicted the decrease in the natural draw ratio and the decrease in draw stress with increasing rubber layer thickness. A more detailed model that includes the bond between the two layers, and the transition zone between the necked and un-necked regions may be able to capture the experiments more quantitatively.

Conflicts of interest

There are no conflicts to declare.

Acknowledgements

We thank Kraton Polymers and Mr Takuya Inaba and Mr Noriyuki Tani from Mitsui Chemicals for making the SEPS and LLDPE films available for this research. This research was supported by the grants NSF-CMMI-1636064 and NSF-CMMI-1561789. S. Hariharakrishnan is grateful to a travel grant from Sastra University, Thanjavur, India, which supported his research.

References

1 T. H. Courtney, *Mechanical Behavior of Materials*, Waveland Press, Illinois, 2nd edn, 1990, ch. 1, pp. 20–30.
2 I. M. Ward, *Mechanical Behavior of Solid Polymers*, J. W. Arrowsmith Ltd, Bristol, 1971, ch. 11, pp. 321–394.
3 A. S. Argon, *The Physics of Deformation and Fracture of Polymers*, Cambridge University Press, Cambridge, U. K., 2013, ch. 10, pp. 325–341.
4 J. W. H. Wallace and H. Carothers, Communication No. 78 from the experimental station of E I Du Pont De Nemours & Co, 1932.
5 I. M. Ward, *Mechanical Properties of Solid Polymers*, W. Arrowsmith Ltd, Bristol, 2nd edn, 1971.
6 P. D. Coates and I. M. Ward, *J. Mater. Sci.*, 1980, **15**, 2897–2914.
7 T. H. Courtney, *Mechanical Behavior of Materials*, Waveland Press, Illinois, 1990.
8 H. A. Kuhn, G. E. Dieter and S. L. Semiatin, *Handbook of Workability and Process Design*, ASM International, United States of America, 2003, ch. 11, p. 147.
9 J. W. Hutchinson and K. W. Neale, *J. Mech. Phys. Solids*, 1983, **31**, 405–426.
10 Y. C. Fung, *Biomechanics Mechanical Properties of Living Tissues*, Springer, 2nd edn, 1993.
11 I. M. Ward, *Mechanical Properties of Solid Polymers*, J. W. Arrowsmith Ltd, England, 1971, ch. 3, pp. 47–55.
12 T. Li and Z. Suo, *Int. J. Solids Struct.*, 2006, **43**, 2351–2363.
13 Y. Xiang, T. Li, Z. G. Suo and J. J. Vlassak, *Appl. Phys. Lett.*, 2005, **87**, 3.
14 F. Maciończyk and W. Bruckner, *J. Appl. Phys.*, 1999, **86**, 4922–4929.
15 T. Li, Z. Y. Huang, Z. C. Xi, S. P. Lacour, S. Wagner and Z. Suo, *Mech. Mater.*, 2005, **37**, 261–273.
16 Z. Y. Xue and J. W. Hutchinson, *Mech. Mater.*, 2007, **39**, 473–487.
17 T. Li and Z. Suo, *Int. J. Solids Struct.*, 2007, **44**, 1696–1705.
18 Z. Y. Xue and J. W. Hutchinson, *Int. J. Solids Struct.*, 2008, **45**, 3769–3778.
19 Z. Jia and T. Li, *Int. J. Plast.*, 2013, **51**, 65–79.
20 Y. Arafat, I. Dutta and R. Panat, *Appl. Phys. Lett.*, 2015, **107**, 5.
21 Y. Arafat, I. Dutta and R. Panat, *J. Appl. Phys.*, 2016, **120**, 11.
22 M. Ben Bettaieb and F. Abed-Meraim, *J. Manuf. Sci. Eng.-Trans. ASME*, 2017, **139**, 10.
23 Y. Q. Liu, K. He, G. Chen, W. R. Leow and X. D. Chen, *Chem. Rev.*, 2017, **117**, 12893–12941.
24 J. Yang, S. Damle, S. Maiti and S. S. Velankar, *Soft Matter*, 2017, **13**, 776–787.
25 S. P. Lacour, D. Chan, S. Wagner, T. Li and Z. G. Suo, *Appl. Phys. Lett.*, 2006, **88**, 3.
26 E. Andreasson, S. Kao-Walter and P. Ståhle, *Eng. Fract. Mech.*, 2014, **127**, 313–326.
27 D. L. Logan, *A first Course in the Finite Element Method*, Thomson, Canada, 2007, ch. 10, pp. 443–484.
28 A. F. Bower, *Applied Mechanics of Solids*, CRC Press, Boca Raton, Florida, 2010, ch. 9, pp. 562–563.
29 R. N. Haward, *Macromolecules*, 1993, **26**, 5860–5869.
30 B. Crist and C. Metaxas, *J. Polym. Sci., Part B: Polym. Phys.*, 2004, **42**, 2081–2091.

